Journal of
Materials Chemistry C

ROYAL SOCIETY
OF CHEMISTRY

PAPER

View Article Online
View Journal | View Issue

Cite this: *J. Mater. Chem. C*, 2024, **12**, 5784

Perovskite quantum dots embedded paper photodetectors with high flexibility and self-powered operation†

Xinwei Guan, ‡[ae] Chien-Yu Huang, ‡*[b] Long Hu,[b] Dharmaraj Periyanagounder,[c] Zhihao Lei,[a] Jiyun Kim,[b] Md. Zahidur Rahaman,[b] Jing-Kai Huang,[d] Prashant Kumar [a] and Chun-Ho Lin *[b]

Metal halide perovskite quantum dots (QDs) with unique physicochemical properties are promising candidates for next-generation optoelectronics, but they often suffer from stability issues that severely limit their potential for practical applications. In this work, we adopt an oleic acid/oleylamine-free approach to synthesize $MAPbBr_3$ quantum dot (MQD) papers by incorporating MQDs into cellulose nanofiber frameworks. The abundant long-chain binding ligands containing sulfate terminal groups within the cellulose nanofiber remarkably stabilize the MQD structure, enabling the fabrication of self-power and flexible MQD paper photodetectors with a responsivity of $\sim$0.19 mA W^{-1}, detectivity of 1.58×10^8 cm $Hz^{1/2}$ W^{-1}, and excellent bendability and reliability after 500 bending cycles. More importantly, these MQD/cellulose-based self-powered photodetectors demonstrate extraordinarily high environmental stability, maintaining more than 90% of the initial responsivity after 60 days. The simple disposability of the paper-based device is also illustrated by burning within one second, suggesting the ease of device elimination. Our work provides a unique approach to designing ultra-stable perovskite QD-based electronics with unprecedented functionalities.

Received 6th February 2024,
Accepted 18th March 2024

DOI: 10.1039/d4tc00508b

rsc.li/materials-c

Introduction

The forthcoming era of wearable electronics and the Internet of Things, which is expected to bring unprecedented innovations to our daily lives, strongly requires smart, flexible electronics with design versatility. One of the key focuses in the development of flexible electronics is the design and production of flexible and stretchable materials that can be used to manufacture the devices.[1] These materials must be able to withstand the rigors of different use conditions while maintaining their electrical and mechanical properties. One prevalent strategy for current commercial flexible electronics is integrating rigid-substrate-based devices with elastomeric carriers.[2] However, this approach could be limited in terms of flexibility, as the individual devices remain rigid and the deformability relies only on the elastomeric carriers. Alternatively, researchers have made significant efforts to develop electronic components on soft substrates to enable highly flexible applications. In this case, the flexibility and mechanical properties of electronic active layers play a dominant role in the device performance and durability, which has become a key research focus in recent years.

Solution-processed hybrid perovskites with a formula of ABX_3 (A = $CH_3NH_3^+$ (MA) and $HC(NH_2)_2^+$ (FA); B = Pb^{2+} and Sn^{2+}; X = Cl^-, Br^-, and I^-) have gained extensive attention in the last decade due to their superior advantages, including narrow emission peaks, ambipolar carrier transport, tunable bandgaps, and long diffusion length.[3–8] Tremendous effort has been devoted to developing next-generation perovskite optoelectronics, witnessing a huge increase in light-to-electricity conversion efficiency up to 26.1% *via* various optimizations within a decade.[9] In the field of flexible electronics, perovskite active layers have been extensively integrated with soft substrates for versatile optoelectronic devices, including photovoltaics,[10,11] light-emitting diodes,[12,13] lasers,[14,15] memristors,[16,17] and photodetectors.[18,19] In particular, metal halide perovskite detectors have been extensively explored in various light detection regions, including

---

[a] *Global Innovative Centre for Advanced Nanomaterials, School of Engineering, Faculty of Engineering and Built Environment, The University of Newcastle, Callaghan, NSW, 2308, Australia*
[b] *School of Materials Science and Engineering, University of New South Wales (UNSW), Sydney, NSW, 2052, Australia. E-mail: chienyu.huang@unsw.edu.au, chun-ho.lin@unsw.edu.au*
[c] *Department of Engineering, University of Cambridge, Cambridge CB3 0FA, UK*
[d] *Department of Materials Science and Engineering, City University of Hong Kong, Hong Kong*
[e] *School of Science, RMIT University, Melbourne, VIC, 3000, Australia*

† Electronic supplementary information (ESI) available. See DOI: https://doi.org/10.1039/d4tc00508b

‡ These authors contributed equally to this work.

near-infrared, visible, ultraviolet, and X/γ-ray detectors, thanks to their exceptional optical and electrical properties.[20] In addition, halide perovskite-based flexible photodetectors have been identified as key components in wearable and portable electronics, benefiting from innovative device architectures and encapsulation strategies to enhance their optoelectronic and mechanical properties.[21] Nevertheless, many reported flexible perovskite devices are based on perovskite polycrystalline films, which are not mechanically robust to fractures along grain boundaries and may hinder their application in highly deformed circumstances.[22]

Zero-dimensional (0D) perovskite quantum dots (QDs), as the rising nanostructure following three-dimensional (3D) bulk perovskites, feature longer carrier diffusion length and higher carrier mobility on account of the improved crystallinity, fewer defects, and grain boundaries compared to bulk polycrystalline thin films.[23] Meanwhile, they can inherit the intrinsic merits of 3D perovskites with additional quantum confinement effects, making them good candidates for wide application in optoelectronic devices.[24] More importantly, the intrinsic nanoscale dimensions of QD materials possess great potential for flexible applications without deteriorating the perovskite materials.[25] However, maintaining good electronic connections between individual QDs under highly deformed conditions is still challenging, which is key to achieving high-endurance flexible QD devices. Another obstacle of perovskite QDs is the poor long-term stability because their ionic lattice might degrade under humidity, temperature, or strong illumination.[26] Currently, most studies on perovskite QD stability focus on the colloidal form. The stability of perovskite QD solid films should be further investigated and enhanced in order to realize practical optoelectronic applications.

In this work, we successfully utilize a facile, room-temperature, solution-processed method to synthesize $MAPbBr_3$ QD (MQD)/cellulose nanofiber (CNF) hybrid papers, elucidating their key optical–electrical properties and demonstrating their potential as self-powered and highly flexible photodetectors. In this design, the flexible CNFs are sulfated by ion exchange treatment to enhance electronic connections between QDs, while the uniformly embedded MQDs serve as excellent optoelectronic media for photo-sensing measurements. Unlike conventional spin-coated perovskite films that typically fracture along grain boundaries during deformation, the sulfated CNFs provide high mechanical strength to support the MQDs, thus enabling highly flexible applications. In addition, the functional sulfate ligands remarkably stabilize the MQD structure, leading to a significant enhancement in the device stability. The resultant hybrid photodetectors demonstrate effective self-power photodetection with a responsivity of ~ 0.19 mA W^{-1}, detectivity of 1.58×10^8 cm $Hz^{1/2}$ W^{-1}, and excellent bendability and reliability after 500 bending cycles, confirming the potential of MQDs/CNF as active flexible electronic components. More importantly, the MQDs/CNF-based self-power photodetectors demonstrate extraordinarily high environmental stability, maintaining more than 90% of the initial responsivity for 60 days.

Results and discussion

CNFs, the ingredients of paper, have dimensions of several hundred nanometers to micrometers in length and several tens nanometers in diameter, originating from a variety of abundant and sustainable biological sources, such as cotton, tunicin, wood pulp, bacteria, and manila.[27–29] By virtue of their high flexibility and mechanical strength, we incorporated high-performance $MAPbBr_3$ perovskite QDs into CNFs to generate flexible optoelectronic sensing films. However, the intrinsic CNFs (I-CNFs) can limit the charge transport between MQDs, leading to insufficient optoelectronic performance. For this reason, we exploited sulfated CNFs (S-CNFs) for nanocomposite design, which are composed of linear polysaccharide chains by repeated β-(1 → 4)-*d*-glucopyranose units while a substantial number of the initial hydroxyl (–OH) groups are substituted by sulfate ($-OSO_3^-$) groups (Fig. 1a) in the ion exchange process. The I-CNFs and S-CNFs were further fabricated and transformed into thin films to test their charge transport properties. It was observed that the conductivity of the S-CNFs increased by 12-fold compared to that of the initial I-CNFs (Fig. S1, ESI†), thus enabling a higher transduction ratio of MQD optoelectronic signals. In addition, the abundant $-OSO_3^-$ groups in the CNFs possess a high electronegativity, and can firmly bind to Pb^{2+} cations on the MQD surface and passivate the defects

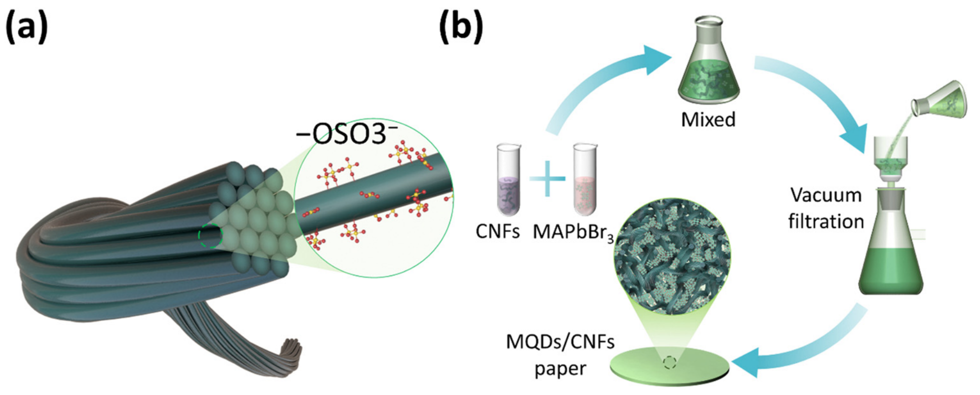

Fig. 1 (a) Illustration of sulfated CNFs. (b) Fabrication of MQDs/CNF papers *via* a vacuum filtration method.

caused by halide vacancies,[30,31] significantly improving the stability and optical properties of MQDs.

In contrast to typical colloidal synthesis, which involves multiple processes to produce high-quality hybrid perovskite QDs, we adopt a different strategy in this study using a simple, oleic acid/oleylamine-free vacuum filtration approach to synthesize the MQD papers, as shown in Fig. 1b.[32] The detailed process can be found in the Experimental section in the ESI.† In short, various amounts of perovskite precursors (MABr : $PbBr_2$ = 1 : 1) and the sulfated CNF suspension were dissolved and mixed in *N*,*N*-Dimethylformamide (DMF). Next, the well-mixed precursor/CNF solutions were vacuum-filtered and dried through a 20-nm pore sized membrane filter for 24 h in order to remove the DMF solvent. Subsequently, MQDs/CNF papers were formed on the membrane and could be easily peeled off. Noteworthily, the rich $-OSO_3^-$ ligands on CNFs effectively confine the $MAPbBr_3$ crystallization into QD structures during the filtering process through ligand-assisted reprecipitation, and the resulting solid-state MQDs/CNF papers are robust and flexible, akin to that of daily used papers.

The morphologies and structures of as-prepared MQDs/CNF papers were characterized by transmission electron microscopy (TEM) and X-ray diffraction (XRD). As shown in Fig. 2a, numerous MQDs are formed as a consequence of ligand confinement and are distributed well in CNF papers. The statistical size distribution of MQDs is shown in Fig. S2 (ESI†), featuring an average size of 6.16 nm (synthesized when perovskite : CNFs = 1 : 10). High-resolution TEM (HRTEM) in Fig. 2b shows the appearance of a single MQD and reveals a lattice spacing of 0.29 nm, which aligns well with the reported value for $MAPbBr_3$ QDs in the literature.[33] Fig. 2c presents the fast Fourier transform (FFT) image corresponding to its (200) plane, confirming the high crystallinity of MQDs. To further confirm the crystal structure of the MQDs/CNF, XRD patterns of bare CNF papers

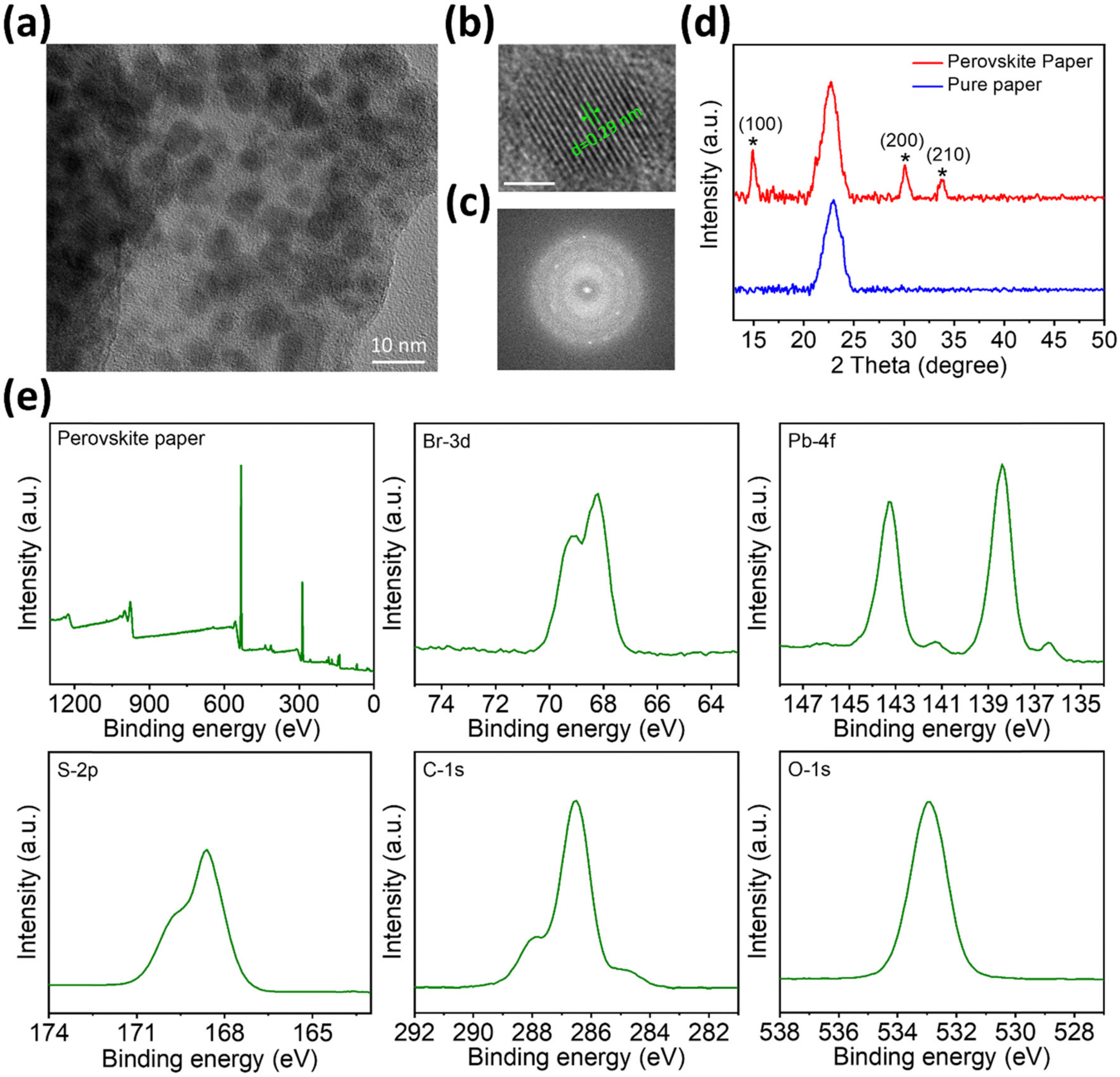

Fig. 2 (a) TEM image of the MQDs/CNF paper. (b) High-resolution TEM image showing the lattice spacing of the $MAPbBr_3$ QD. The scale bar is 2 nm. (c) Corresponding electron diffraction pattern, revealing the high crystallinity of the perovskite QDs. (d) XRD patterns of pure CNF and MQDs/CNF papers. (e) Full XPS spectrum and Br-3d, Pb-4f, S-2p, C-1s, O-1s core spectra of MQDs/CNF papers.

and MQDs/CNF hybrid papers were measured (Fig. 2d). Both samples show a strong peak at 22.6°, ascribed to the (200) plane of the CNF paper.[31] Notably, three extra peaks were observed in MQDs@20/CNF at 14.9°, 30.1°, and 33.8°, corresponding to the (100), (200), and (210) planes of MQDs, respectively.[13,32] The TEM and XRD results suggest the successful embedding of MQDs into CNF papers. The full X-ray photoelectron spectroscopy (XPS) spectrum and Br-3d, Pb-4f, S-2p, C-1s, and O-1s core spectra of MQDs/CNF were also recorded, as shown in Fig. 2e. The XPS results confirm the binding energies of molecular interaction in MQDs/CNF, and the presence of the S-2p peak also suggests the potential capping effect from ($-OSO_3^-$) terminal groups in the hybrid structure.

To optimize the optical and electrical properties of MQDs/CNF hybrid papers, three varied loading amounts of perovskite precursors and CNFs with weight ratios of 10%, 20%, and 30% were prepared (*i.e.*, MQDs@10/CNF, MQDs@20/CNF, and MQDs@30/CNF). Fig. 3a shows the optical image of MQDs/CNF papers with different MQD concentrations, illustrating the progressive color evolution in their appearance. The bare CNF paper has a grey color; with the concentration of MQDs gradually increasing from 10% to 30%, the color of MQDs/CNF papers turns from light green-yellow to deep orange. The surface morphologies of different MQDs/CNF papers were studied using a Zygo profilometer, as shown in Fig. S3 (ESI†). These hybrid papers gradually become rougher as the MQD concentration increases, with the root mean square (RMS) roughness values of 450, 495, 511, and 562 nm for bare CNF, MQDs@10/CNF, MQDs@20/CNF, and MQDs@30/CNF, respectively, suggesting that higher concentrations of MQDs can alter the hybrid paper morphology. Moreover, the top-view scanning electron microscopy (SEM) images in Fig. 3b exhibit a rougher morphology in the MQDs@30/CNF paper than the other two, which is consistent with the above results. Since a higher percentage of perovskite precursors can presumably lead to extra crystallization on the surface of the CNF paper, a certain amount of perovskite crystals could float on the surface of the hybrid paper without the protection of the CNF. The precipitated crystal was confirmed to be $MAPbBr_3$ by SEM energy dispersive X-ray spectroscopy (EDX), as shown in Fig. S4 (ESI†). Therefore, the stability of MQDs@30/CNF is expected to be lower than those of MQDs@20/CNF and MQDs@10/CNF.

Ultraviolet-visible (UV-Vis) absorption spectra of different perovskite papers were recorded, as shown in Fig. 3c. The MQDs@30/CNF sample showed a steep absorption onset around 553 nm, close to values reported for the bulk $MAPbBr_3$ perovskite. The absorption onset is slightly blue-shifted for MQDs@20/CNF, while for MQDs@10/CNF, the absorption onset shifted by over 20 nm, suggesting a much stronger quantum confinement due to the smaller QD size for this sample. The steady-state photoluminescence (PL) characteristics of MQDs/CNF papers are demonstrated in Fig. 3d. The reported polycrystalline $MAPbBr_3$ thin film typically has a PL peak at >530 nm,[34] which is obviously larger than for our MQDs/CNF papers, indicating that the involved quantum confinement effect alters the bandgaps of MQDs on CNF papers. Notably, a systematic blue shift can be observed as the concentration of MQDs decreases due to the enhanced degree of quantum confinement. Time-resolved PL (TRPL) of different MQDs/CNF papers was used to verify their photoexcited carrier

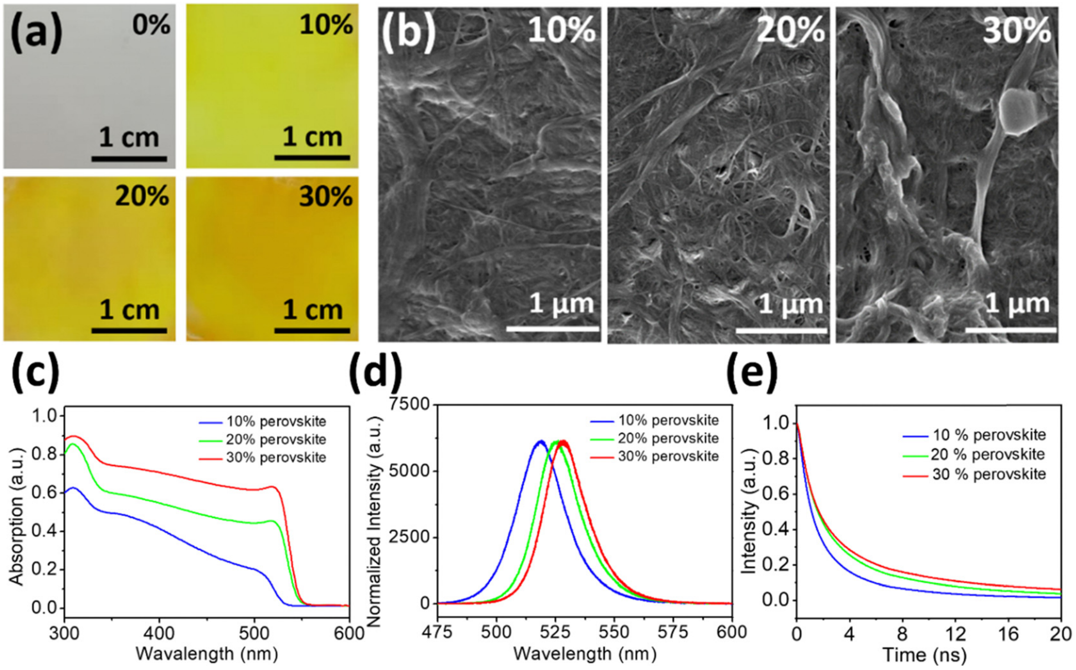

Fig. 3 (a) Optical photographs of MQDs/CNF papers with different perovskite concentrations from 0%, 10%, 20%, to 30%. (b) Top-view SEM images of MQDs/CNF papers with 10%, 20%, and 30% perovskite concentrations. (c) UV-Vis absorption, (d) PL, and (e) TRPL spectra of three different MQDs/CNF papers.

dynamics (Fig. 3e). By conducting the exponential fitting, the TRPL average carrier lifetimes are determined to be 2.24 ns, 3.38 ns, and 3.80 ns for MQDs@10/CNF, MQDs@20/CNF, and MQDs@30/CNF, respectively. The decrease in carrier lifetime with lower MQD concentrations can be attributed to the increase in the carrier recombination rate resulting from enhanced quantum confinement, which matches the observations in UV-Vis and PL studies.

The potential of MQDs/CNF hybrid papers with excellent mechanical strength and impressive optoelectronic properties draws our attention and inspires us to study their performance for self-biased photodetectors. It is worth noting that all the measurements were conducted at room temperature (20 °C) under ambient conditions with a humidity of 60%. The self-powered Schottky photodetector can be achieved by planarly sandwiching the MQDs/CNF hybrid paper between one Au and one Pt electrode. This Schottky design has been proven quite effective for perovskite materials in the previous study.[35] We first conducted the *I–V* measurement of MQDs@10/CNF under dark conditions, and an extremely small current of around 1.05 nA was observed at 0 V (Fig. 4a, the corresponding semilog plot is shown in Fig. S5, ESI†). Remarkably, under solar light irradiation of 100 mW cm^{-2}, the zero-bias photocurrent significantly increases by 212 times to >0.2 μA. Because Au and Pt feature high work functions of 5.6 eV and 5.1 eV, respectively, they can facilitate the p-type transport of $\mathrm{MAPbBr_3}$ QDs.[36] The band diagram of Au/$\mathrm{MAPbBr_3}$/Pt is shown in Fig. S6 (ESI†), in which the Pt/$\mathrm{MAPbBr_3}$ interface has a small barrier, while Au/$\mathrm{MAPbBr_3}$ exhibit a larger Schottky interface,[36] demonstrating a Schottky-typed self-powered mechanism. When photoexcited carriers are generated, the holes tend to transport to the Au contact due to the potential difference, facilitating the self-powered photodetection. The rectifying *I–V* behavior in Fig. 4a also confirms the carrier transport to be a Schottky-typed self-powered mechanism. The temporal response of the MQDs@10/CNF photodetector in Fig. 3b illustrates the fast photocurrent switching, with a rise time of 290 ms (current increasing from 10% to 90% of the peak value) and a decay time of 510 ms (current decreasing from 90% to 10% of the peak value). The decay of photocurrent is relatively slower than the rise, presumably owing to the large channel length of ∼400 μm and charge-trapping centers at the MQDs/CNF interface.

In order to further investigate the effect of perovskite QD concentration on photodetector performance, three types of MQDs/CNF hybrid paper-based devices were fabricated, including MQDs@10/CNF, MQDs@20/CNF, and MQDs@30/CNF. Fig. 5a depicts the time-dependent photocurrent responses of three photodetectors under zero bias, recorded as the solar light illumination was cycled on and off at two-second intervals. It is clear that with more MQD incorporation inside the CNF paper, the photocurrent increased significantly from 5.6×10^{-8} A for MQDs@10/CNF to 1.8×10^{-7} A for MQDs@20/CNF and 3.2×10^{-7} A for MQDs@30/CNF. However, their dark currents are also increased accordingly because of increased interfacial charge transfer and carrier-donating defects with a higher MQD density. To this end, MQDs@20/CNF demonstrates the highest ON/OFF ratio of 40.

The photoresponsivity (R) was calculated as $R = \dfrac{I_{\mathrm{on}} - I_{\mathrm{off}}}{P \times A}$, where $I_{\mathrm{on}} - I_{\mathrm{off}}$ is the difference between the photocurrent and the dark current, P is the power intensity of incident light, and A is the irradiation area of the device. Since the photocurrent enhances as the perovskite concentration increases, the MQDs@30/CNF presents the highest peak responsivity of 0.19 mA W^{-1} (Fig. 5b), which is higher compared to the MQDs@20/CNF (0.12 mA W^{-1}) and MQDs@10/CNF (0.03 mA W^{-1}), respectively. Detectivity (D^*) is a crucial performance indicator for assessing the sensitivity of photodetectors. Herein, the detectivity of different MQDs/CNF photodetectors in self-powered mode (0 V) is calculated by $D^* = R/(2eJ_{\mathrm{d}})^{1/2}$, where e is the elementary charge and J_{d} is the current density under dark conditions. The MQDs@10/CNF photodetector features a detectivity of 5.64×10^7 cm Hz$^{1/2}$ W^{-1}, compared with the MQDs@20/CNF (1.58×10^8 cm Hz$^{1/2}$ W^{-1}) and MQDs@30/CNF (7.30×10^7 cm Hz$^{1/2}$ W^{-1}) counterparts, as demonstrated in Fig. 5c. Even though the reduction in perovskite concentration within the MQDs/CNF would slightly suppress the responsivity, the corresponding lower dark current can substantially diminish the background noise, leading to a comparable detectivity.

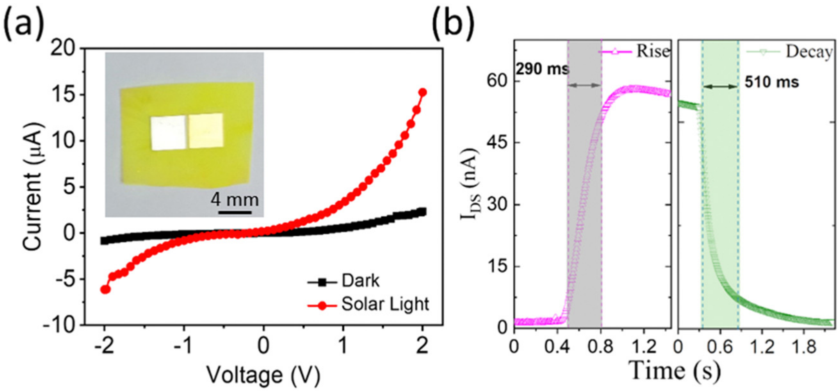

Fig. 4 (a) *I–V* curves of Au/MQDs@10/CNF/Pt under dark and solar light illumination. The inset shows the photograph of the Au/MQDs@10/CNF/Pt device. (b) Temporal photocurrent responses highlight a rise time of 290 ms and a decay time of 510 ms.

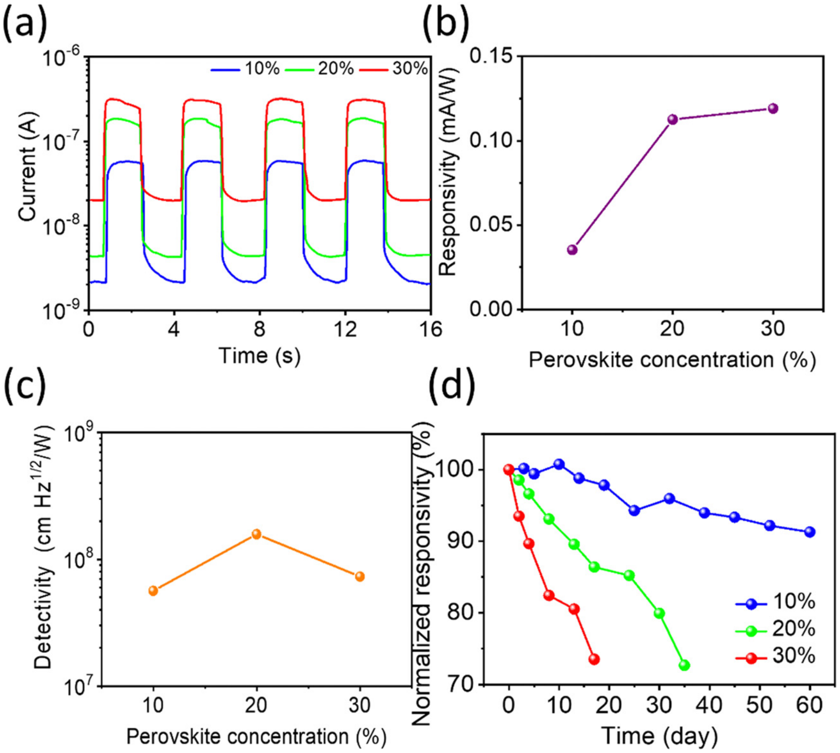

Fig. 5 (a) Self-powered photocurrent responses of three perovskite concentration MQDs/CNF photodetectors showing time-dependent photosensitivity with a time interval of 2 s, and their corresponding photoresponsivity and detectivity are shown in (b) and (c). (d) Time-dependent normalized photoresponsivity of MQDs/CNF photodetectors under relative humidity of 60% at 20 °C.

Stability is an important parameter for halide perovskite devices. In this study, the stability of different MQDs/CNF photodetectors was determined by measuring the responsivity with time under a relative humidity of 60% at 20 °C, as shown in Fig. 5d. Impressively, MQDs@10/CNF can sustain more than 91% of the initial responsivity even after 60 days, demonstrating its superior stability. In contrast, it takes 35 days for MQDs@20/CNF to reach 73% of its initial responsivity and 17 days for MQDs@30/CNF to degrade to 73.5%. It is verified that the slightly higher responsivity and detectivity of MQDs@20/CNF and MQDs@30/CNF are at significant expense of stability performance. Therefore, with comparable detectivity and excellent stability, MQDs@10/CNF shows better potential for reliable self-powered photodetection. To further test the repeatability, the responsivity of the MQDs@10/CNF paper photodetector was tested 20 times, and five MQDs@10/CNF devices were fabricated to determine the uniformity and the statistical results are summarized in Table S1 (ESI†).

To understand the effect of CNFs in the hybrid structure, the stability of a pure MQD thin film device was also tested for comparison (Fig. S7, ESI†). Without CNFs, the photocurrent of the pure MQD device was rapidly degraded to 67.1% within 4 days, which is significantly inferior to the MQDs/CNF counterpart. The excellent stability of the MQDs/CNF hybrid structure can be attributed to the molecular interaction. CNFs, exhibiting substantial mechanical robustness and an intricate entanglement of cellulose fibers, have been identified as efficacious natural crosslinking agents,[37] which can enhance the structural integrity and durability of MQD papers. The CNFs utilized in this study contain abundant highly electronegative sulfonate ($-HSO_3^-$) capping ligands. Such ligands demonstrate a pronounced affinity for complexation with the cationic species within the MQDs, specifically lead ions (Pb^{2+}). This interaction substantially improves the stability of the MQDs, leveraging the inherent functionality of CNFs to foster enhanced performance and high stability of the MQDs. To further investigate its interaction with Pb^{2+}, the XPS Pb-4f core spectra of both MQDs/CNF and pure MQDs were characterized, respectively (Fig. S8, ESI†). It is observed that the Pb-4$f_{7/2}$ and Pb-4$f_{5/2}$ peaks of MQDs/CNF slightly shift to lower binding energy compared to those of the pure MQDs. This result confirms the interaction between CNFs and MQDs because the electron-rich capping ligands can bond to Pb^{2+}, producing an electron screening effect that shifts the binding energy to lower values.[38] The capping effect of CNFs can significantly stabilize the MQDs, leading to the enhanced stability of MQDs/CNF compared to that of conventional oleic acid/oleylamine synthesized MQDs.

In this study, the performance of MQDs/CNF photodetectors is substantially correlated to the perovskite to CNF weight ratios, which results in different QD sizes. The MQDs@10/CNF exhibits an average QD size of 6.16 nm (Fig. 2a and Fig. S2, ESI†), while MQDs@20/CNF features a much larger average QD size of 9.31 nm (Fig. S9, ESI†). Moreover, when the perovskite to CNF ratio further increases to 30% for MQDs@30/CNF (Fig. S10, ESI†), the perovskite grain is significantly enlarged without clear boundaries and a certain amount

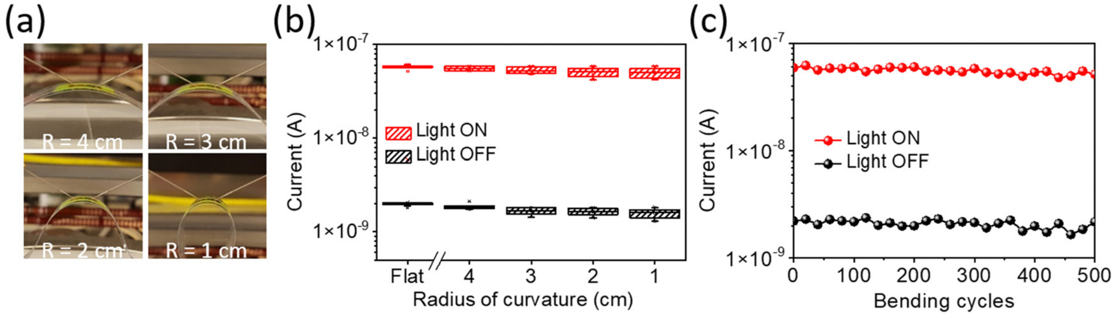

Fig. 6 (a) Photograph of the flexible MQDs@10/CNF paper photodetector under different bending conditions. (b) I_{on} and I_{off} of the MQDs@10/CNF photodetector measured with various bending curvature from flat, 4, 3, 2, to 1 cm. (c) Endurance characterization of the MQDs@10/CNF device.

of large perovskite crystals appear on the paper surface. Photodetector performance results based on different MQDs/CNF papers (Fig. 5) suggest that the responsivity increases when the perovskite concentration increases as a result of enhanced light absorption by larger MQDs. However, the detectivity of different photodetectors remains at a similar level because larger MQDs also lead to increased noise (dark current), balancing the positive effect of enhanced responsivity. For the stability test in Fig. 5d, when the perovskite concentration and crystal size increase in the cellulose paper, the capping effect of CNFs would reduce accordingly, leading to a decrease in photodetector stability. As a result, the MQDs@10/CNF paper photodetector possesses the best stability, exhibiting great potential for self-powered photodetection.

The paper-based flexible optoelectronics have drawn significant attention recently because of the extended market demand for wearable and foldable consumer electronics.[39] To verify the application of the MQDs/CNF hybrid paper in flexible electronics, a bending test was performed to examine whether it could reliably function under bent conditions. As depicted in Fig. 6a, four degrees of bending were studied with the radius of curvature (r) between two edges of the substrate from 4, 3, 2, to 1 cm. Compared to operation under flat conditions, despite slightly increasing fluctuation, both photocurrent and dark current levels remained nearly unchanged at four different bending states (Fig. 6b), indicating good flexibility of the MQDs@10/CNF photodetector. To further test the mechanical robustness, the photodetector performances were monitored continuously over repetitive bending cycles. Specifically, each data point was obtained by subjecting the devices to 20 bending cycles, alternating between a flat state and a curvature of 1 cm bending radius, as illustrated in Fig. 6c, in which a stable photodetector performance was observed even after 500 bending cycles. The excellent device stability after successive bending confirms the reliability of the flexible MQDs/CNF paper photodetector.

An additional advantage of MQDs/CNF paper devices is the ability to be easily modified in size and shape using scissors by cutting and trimming. Unlike other flexible devices constructed on traditional polymer substrates, the capability of adjusting size and shape could greatly enhance the customization of MQDs/CNF to meet individual requirements. Employing kirigami techniques also allows for the creation of a wide range of intricate patterns, adding aesthetic value. In addition, MQDs/CNF paper-based devices can be easily disposed of, in which the whole device can be irreversibly and totally wiped out by burning *via* a commercial lighter. As demonstrated in Fig. 7, the paper-based photodetector quickly darkens and decomposes within 0.5 s, resulting in the permanent elimination of the device. Notably, the cellulose paper will not deform and generate toxic gases like low-cost plastics upon burning, so it is relatively environmentally friendly for flexible electronic applications.

Table 1 summarises the performance of the MQDs/CNF photodetectors in this work and other perovskite-based self-powered photodetectors in the literature.[35,40–50] It can be seen that although the detectivity of MQDs/CNF is slightly lower, their stability is significantly better than in other reports,

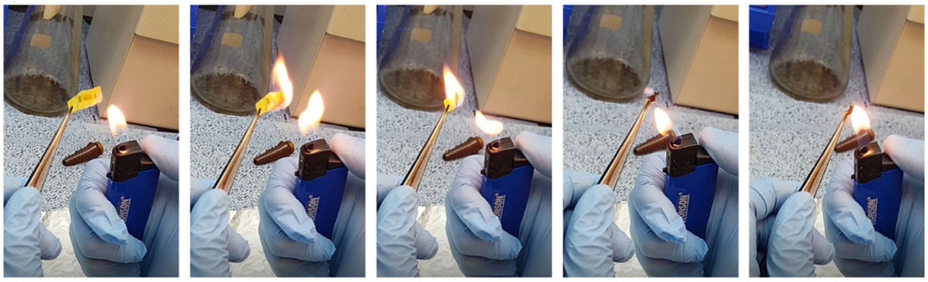
0 s 0.125 s 0.25 s 0.375 s 0.5 s

Fig. 7 Time-lapse sequence of photographs showing the ignition process of the MQDs/CNF paper photodetector within 0.5 s.

Table 1 Comparison of perovskite-based self-powered photodetectors

Device structure	Wavelength (nm)	Responsivity [mA W^{-1}]	Detectivity [Jones]	Response time [ms]	Stability	Flexible	Ref.
Au/$CsPbBr_3$/Pt	550	28	1.7×10^{11}	230/60 ms	50 min	No	35
FTO/TiO_2/$MAPbI_3$–carbon	White light	1.3	8.2×10^{11}	200/500 ms	N/A	No	40
FTO/TiO_2/$CsPbBr_3$/carbon	520	350	1.94×10^{13}	0.58 μs	N/A	No	41
AMP$(MA)_2Pb_3Br_{10}$/$MAPbBr_3$	405	1.5	3.8×10^{10}	600 μs	30 days	No	42
Al/$MAPbI_3$/Au	808	from 10^{-5} to 38	N/A	71/112 μs	N/A	No	43
ITO/NiO_x/$FAPbBr_3$/Ag	450	123.6	7.1×10^{11}	10/200 ns	400 s	No	44
Au/$FAPbBr_3$/Au	397	0.18	1.6×10^{8}	N/A	N/A	No	45
Au/$MAPbI_3$/Au	300	2.2	1.76×10^{11}	27.2/26.2 ms	N/A	Yes	46
Ag/spiro/$MAPbI_3$/In_2O_3/ITO	720	451	1.1×10^{11}	200 ms	90% after 800 s	Yes	47
Ni/$MAPbI_3$/Al	532	227	1.36×10^{11}	61/42 ms	N/A	Yes	48
C/TiO_2/$MAPbI_3$-spiro/Au	550	16.9	1.1×10^{10}	200 ms	$<$70% after 8500 s	Yes	49
Graphene/ZnO/$MAPbI_3$/PTAA/Au	700	343	5.82×10^{9}	1.85/1.02 μs	N/A	Yes	50
Au/MQDs/CNF/Pt	Solar light	0.19	1.58×10^{8}	290/510 ms	$>$90% after 60 days	Yes	This work

demonstrating the effectiveness of the CNF capping strategy to confine and stabilize the MQDs. It should be noted that perovskite photodetectors typically present much better responsivity and detectivity under weak light conditions. For example, in Ding *et al.*'s work,[43] the responsivity of the perovskite photodetector was enhanced by more than 100 times from $\sim$0.3 mA W^{-1} to $\sim$40 mA W^{-1} when the illumination intensity decreases from 10 mW cm^{-2} to 10^{-3} mW cm^{-2}. In this study, the MQDs/CNF photodetectors were tested under strong solar light of 100 mW cm^{-2}, and therefore, the obtained performance should be underestimated. Combined with high flexibility and exceptional stability, MQDs/CNF show great potential for self-powered photodetection in flexible applications.

Conclusions

In summary, we propose a novel and facile strategy for fabricating flexible halide perovskite-based self-powered optoelectronics and significantly enhancing their environmental stability. By incorporating 0D MQDs into cellulose nanofiber papers, a flexible MQDs/CNF hybrid paper photodetector is developed, featuring effective self-power photodetection with a responsivity of $\sim$0.19 mA W^{-1}, detectivity of 1.58×10^{8} cm $Hz^{1/2}$ W^{-1}, and great bendability and reliability with reproducible photodetection over 500 bending cycles. In addition, MQDs/CNF-based self-powered photodetectors demonstrate extraordinarily high environmental stability, which retains more than 90% of the initial responsivity for 60 days owing to the abundant long-chain binding ligands that stabilize and protect the MQD structure. The ease of disposing of paper-based photodetectors is evidenced by their ability to be completely incinerated within a single second, highlighting a straightforward method for device disposal. Our research opens new avenues for the development of exceptionally stable, paper-based electronics incorporating halide perovskite QDs, offering superior optoelectronic functionalities for highly flexible, self-powered applications.

Conflicts of interest

The authors declare no conflicts of interest.

Acknowledgements

X. G. and C.-Y. H. contributed equally to this work. X. G. and P. K. acknowledge the financial support from the University of Newcastle. L. H. acknowledges the support from the Australian Research Council (DE230101711).

References

1 X. Chen, J. A. Rogers, S. P. Lacour, W. Hu and D.-H. Kim, *Chem. Soc. Rev.*, 2019, **48**, 1431–1433.

2 S. Biswas, A. Schoeberl, Y. Hao, J. Reiprich, T. Stauden, J. Pezoldt and H. O. Jacobs, *Nat. Commun.*, 2019, **10**, 4909.

3 C.-Y. Huang, H. Li, Y. Wu, C.-H. Lin, X. Guan, L. Hu, J. Kim, X. Zhu, H. Zeng and T. Wu, *Nano-Micro Lett.*, 2022, **15**, 16.

4 C. Liu, K. Wang, C. Yi, X. Shi, P. Du, A. W. Smith, A. Karim and X. Gong, *J. Mater. Chem. C*, 2015, **3**, 6600–6606.

5 P. R. Anandan, M. Nadeem, C.-H. Lin, S. Singh, X. Guan, J. Kim, S. Shahrokhi, M. Z. Rahaman, X. Geng, J.-K. Huang, H. Nguyen, H. Hu, P. Sharma, J. Seidel, X. Wang and T. Wu, *Appl. Phys. Rev.*, 2023, **10**, 041312.

6 J. Miao and F. Zhang, *J. Mater. Chem. C*, 2019, **7**, 1741–1791.

7 T. Yang, F. Li, C.-H. Lin, X. Guan, Y. Yao, X. Yang, T. Wu and R. Zheng, *Cell Rep. Phys. Sci.*, 2023, **4**, 101447.

8 L. Hu, X. Guan, T. Wan, C.-H. Lin, S. Liu, R. Zhu, W. Chen, Y. Yao, C.-Y. Huang, L. Yuan, S. Shahrokhi, D. Chu, C. Cazorla, J. Chen, J. Yang, J. Yi, S. Huang and T. Wu, *ACS Energy Lett.*, 2022, **7**, 4150–4160.

9 H. Min, D. Y. Lee, J. Kim, G. Kim, K. S. Lee, J. Kim, M. J. Paik, Y. K. Kim, K. S. Kim and M. G. Kim, *Nature*, 2021, **598**, 444–450.

10 Q. Luo, H. Ma, Q. Hou, Y. Li, J. Ren, X. Dai, Z. Yao, Y. Zhou, L. Xiang, H. Du, H. He, N. Wang, K. Jiang, H. Lin, H. Zhang and Z. Guo, *Adv. Funct. Mater.*, 2018, **28**, 1706777.

11 L. Yang, J. Feng, Z. Liu, Y. Duan, S. Zhan, S. Yang, K. He, Y. Li, Y. Zhou, N. Yuan, J. Ding and S. Liu, *Adv. Mater.*, 2022, **34**, 2201681.

12 D. H. Jung, J. H. Park, H. E. Lee, J. Byun, T. H. Im, G. Y. Lee, J. Y. Seok, T. Yun, K. J. Lee and S. O. Kim, *Nano Energy*, 2019, **61**, 236–244.

13 C. Y. Kang, C. H. Lin, C. H. Lin, T. Y. Li, S. W. Huang Chen, C. L. Tsai, C. W. Sher, T. Z. Wu, P. T. Lee and X. Xu, *Adv. Sci.*, 2019, **6**, 1902230.

14 H. Zhang, Q. Liao, X. Wang, J. Yao and H. Fu, *Adv. Opt. Mater.*, 2016, **4**, 1718–1725.

15 Y.-C. Wang, H. Li, Y.-H. Hong, K.-B. Hong, F.-C. Chen, C.-H. Hsu, R.-K. Lee, C. Conti, T. S. Kao and T.-C. Lu, *ACS Nano*, 2019, **13**, 5421–5429.

16 C. Gu and J.-S. Lee, *ACS Nano*, 2016, **10**, 5413–5418.

17 D. Liu, Q. Lin, Z. Zang, M. Wang, P. Wangyang, X. Tang, M. Zhou and W. Hu, *ACS Appl. Mater. Interfaces*, 2017, **9**, 6171–6176.

18 S.-F. Leung, K.-T. Ho, P.-K. Kung, V. K. S. Hsiao, H. N. Alshareef, Z. L. Wang and J.-H. He, *Adv. Mater.*, 2018, **30**, 1704611.

19 M. T. Vijjapu, M. E. Fouda, A. Agambayev, C. H. Kang, C.-H. Lin, B. S. Ooi, J.-H. He, A. M. Eltawil and K. N. Salama, *Light: Sci. Appl.*, 2022, **11**, 3.

20 Y. Chen, Z. Feng, A. Pal and J. Zhang, *Phys. Status Solidi A*, 2022, **219**, 2200018.

21 Y. Wang, D. Li, L. Chao, T. Niu, Y. Chen and W. Huang, *Appl. Mater. Today*, 2022, **28**, 101509.

22 J. Zhao, L. Zhao, Y. Deng, X. Xiao, Z. Ni, S. Xu and J. Huang, *Nat. Photonics*, 2020, **14**, 612–617.

23 K. Hong, Q. V. Le, S. Y. Kim and H. W. Jang, *J. Mater. Chem. C*, 2018, **6**, 2189–2209.

24 J. Kim, A. T. John, H. Li, C.-Y. Huang, Y. Chi, P. R. Anandan, K. Murugappan, J. Tang, C.-H. Lin, L. Hu, K. Kalantar-Zadeh, A. Tricoli, D. Chu and T. Wu, *Small Methods*, 2024, **8**, 2300417.

25 L. Hu, Q. Zhao, S. Huang, J. Zheng, X. Guan, R. Patterson, J. Kim, L. Shi, C.-H. Lin, Q. Lei, D. Chu, W. Tao, S. Cheong, R. D. Tilley, A. W. Y. Ho-Baillie, J. M. Luther, J. Yuan and T. Wu, *Nat. Commun.*, 2021, **12**, 466.

26 A. Younis, C. H. Lin, X. Guan, S. Shahrokhi, C. Y. Huang, Y. Wang, T. He, S. Singh, L. Hu and J. R. D. Retamal, *Adv. Mater.*, 2021, **33**, 2005000.

27 C.-H. Lin, H.-C. Fu, B. Cheng, M.-L. Tsai, W. Luo, L. Zhou, S.-H. Jang, L. Hu and J.-H. He, *npj 2D Mater. Appl.*, 2018, **2**, 1–6.

28 J. Gong, J. Li, J. Xu, Z. Xiang and L. Mo, *RSC Adv.*, 2017, **7**, 33486–33493.

29 J. Guo, D. Liu, I. Filpponen, L.-S. Johansson, J.-M. Malho, S. Quraishi, F. Liebner, H. A. Santos and O. J. Rojas, *Biomacromolecules*, 2017, **18**, 2045–2055.

30 D. Yang, X. Li, W. Zhou, S. Zhang, C. Meng, Y. Wu, Y. Wang and H. Zeng, *Adv. Mater.*, 2019, **31**, 1900767.

31 C.-H. Chiang, T.-Y. Li, H.-S. Wu, K.-Y. Li, C.-F. Hsu, L.-F. Tsai, P.-K. Yang, Y.-J. Lee, H.-C. Lee and C.-Y. Wang, *Nanotechnology*, 2020, **31**, 324002.

32 T.-Y. Li, X. Xu, C.-H. Lin, X. Guan, W.-H. Hsu, M.-L. Tsai, X. Fang, T. Wu and J.-H. He, *Adv. Sci.*, 2020, **7**, 1902439.

33 E. T. Vickers, E. E. Enlow, W. G. Delmas, A. C. DiBenedetto, A. H. Chowdhury, B. Bahrami, B. W. Dreskin, T. A. Graham, I. N. Hernandez, S. A. Carter, S. Ghosh, Q. Qiao and J. Z. Zhang, *ACS Energy Lett.*, 2020, **5**, 817–825.

34 B. Wu, H. Yuan, Q. Xu, J. A. Steele, D. Giovanni, P. Puech, J. Fu, Y. F. Ng, N. F. Jamaludin, A. Solanki, S. Mhaisalkar, N. Mathews, M. B. J. Roeffaers, M. Grätzel, J. Hofkens and T. C. Sum, *Nat. Commun.*, 2019, **10**, 484.

35 M. I. Saidaminov, M. A. Haque, J. Almutlaq, S. Sarmah, X.-H. Miao, R. Begum, A. A. Zhumekenov, I. Dursun, N. Cho, B. Murali, O. F. Mohammed, T. Wu and O. M. Bakr, *Adv. Opt. Mater.*, 2017, **5**, 1600704.

36 C.-H. Lin, L. Hu, X. Guan, J. Kim, C.-Y. Huang, J.-K. Huang, S. Singh and T. Wu, *Adv. Mater.*, 2022, **34**, 2108616.

37 X. Guan, P. Kumar, Z. Li, T. K. A. Tran, S. Chahal, Z. Lei, C.-Y. Huang, C.-H. Lin, J.-K. Huang, L. Hu, Y.-C. Chang, L. Wang, J. S. J. Britto, L. Panneerselvan, D. Chu, T. Wu, A. Karakoti, J. Yi and A. Vinu, *Adv. Sci.*, 2023, **10**, 2205809.

38 J. Zhang, X. Liu, P. Jiang, H. Chen, Y. Wang, J. Ma, R. Zhang, F. Yang, M. Wang, J. Zhang and G. Tu, *Nano Energy*, 2019, **66**, 104142.

39 H. Shen, S. Peng, Q. Luo, J. Zhou, J.-H. He, G. Zhou and X. Xu, *Adv. Funct. Mater.*, 2023, **33**, 2213820.

40 S. Murali, S. P. Madhusudanan, A. K. Pathak, P. M. Jayasankar and S. K. Batabyal, *Mater. Lett.*, 2019, **254**, 428–432.

41 W. Zhu, M. Deng, Z. Zhang, D. Chen, H. Xi, J. Chang, J. Zhang, C. Zhang and Y. Hao, *ACS Appl. Mater. Interfaces*, 2019, **11**, 22543–22549.

42 X. Zhang, L. Li, C. Ji, X. Liu, Q. Li, K. Zhang, Y. Peng, M. Hong and J. Luo, *Natl. Sci. Rev.*, 2021, **8**, nwab044.

43 J. Ding, H. Fang, Z. Lian, J. Li, Q. Lv, L. Wang, J.-L. Sun and Q. Yan, *CrystEngComm*, 2016, **18**, 4405–4411.

44 K. Tao, C. Xiong, J. Lin, D. Ma, S. Lin, B. Wang and H. Li, *Adv. Electron. Mater.*, 2023, **9**, 2201222.

45 S.-T. Dong, Z. Fu, M. Yu, J.-L. Jiang, X. Jin, Y.-H. Guo, L. Wang and Y.-M. Zhang, *CrystEngComm*, 2022, **24**, 2100–2106.

46 S. Lim, M. Ha, Y. Lee and H. Ko, *Adv. Opt. Mater.*, 2018, **6**, 1800615.

47 M. Wang, F. Cao, L. Meng, W. Tian and L. Li, *Adv. Mater. Interfaces*, 2019, **6**, 1801526.

48 J. Tao, Z. Xiao, J. Wang, C. Li, X. Sun, F. Li, X. Zou, G. Liao and Z. Zou, *J. Alloys Compd.*, 2020, **845**, 155311.

49 H. Sun, T. Lei, W. Tian, F. Cao, J. Xiong and L. Li, *Small*, 2017, **13**, 1701042.

50 D. H. Shin, J. S. Ko, S. K. Kang and S.-H. Choi, *ACS Appl. Mater. Interfaces*, 2020, **12**, 4586–4593.